Tuning the Relative Stability and Reactivity of Manganese Dioxygen and Peroxo Intermediates via Systematic Ligand Modification

Published as part of the Accounts of Chemical Research special issue "Synthesis in Biological Inorganic Chemistry".

Julie A. Kovacs*

The Department of Chemistry, University of Washington, Box 351700, Seattle, Washington 98195-1700, United States

CONSPECTUS: Many fundamental processes of life depend on the chemical energy stored in the O−O bond of dioxygen (O_2), the majority of which is derived from photosynthetic H_2O oxidation. Key steps in these processes involve Mn-, Fe-, or Cu-promoted formation or cleavage of O−O and O−H bonds, the mechanisms of which are not fully understood, especially with Mn. Metal−peroxo and high-valent metal−oxo species are proposed to be involved as intermediates. The metal ion properties that favor O−O and O−H bond formation versus cleavage have yet to be systematically explored. Herein we examine the O_2 reactivity of a series of

structurally related Mn(II) complexes and show that several metastable intermediates are observed, the relative stabilities of which depend on subtle differences in ligand architecture. We show that in contrast to Fe and Cu complexes, O_2 binds irreversibly to Mn(II). By crystallizing an entire series of the first reported examples of Mn(III)−OOR peroxos as well as an O_2-derived binuclear *trans-μ*-1,2-bridged Mn(III)−peroxo with varying degrees of O−O bond activation, we demonstrate that there are distinct correlations between spectroscopic, structural, and reactivity properties. Rate-limiting O−O bond cleavage is shown to afford a reactive species capable of abstracting H atoms from 2,4-^{t}Bu$_2$-PhOH or 1,4-cyclohexadiene, depending on the ligand substituents. The weakly coordinated N-heterocycle Mn···N^{py,quino} distance is shown to correlate with the peroxo O−O bond length and modulate the π overlap between the filled π_v^*(O−O) and Mn d_{xz} orbitals. We also show that there is a strong correlation between the peroxo → Mn charge transfer (CT) band and the peroxo O−O bond length. The energy difference between the CT bands associated with the peroxos possessing the shortest and longest O−O bonds shows that these distances are spectroscopically distinguishable. We show that we can use this spectroscopic parameter to estimate the O−O bond length, and thus the degree of O−O bond activation, in intermediates for which there is no crystal structure, as long as the ligand environment is approximately the same.
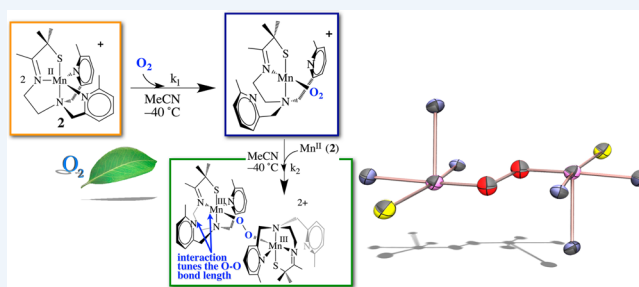
INTRODUCTION

The energy stored in the O−O bond of O_2 sustains aerobic life by driving essential metabolic and biosynthetic pathways, including DNA synthesis and repair[1] and the biosynthesis of neurotransmitters[2] and hormones.[2] Manganese-, iron-, and copper-containing enzymes catalyze the majority of these reactions.[2−8] Although O_2-mediated oxidation reactions are thermodynamically favored, they are spin-forbidden and thus kinetically slow unless promoted by a transition-metal ion.[9] Most of the O_2 on our planet is generated via Mn-promoted H_2O splitting.[4,10,11] The formation and/or cleavage of O−O and O−H bonds represent key steps in dioxygen activation, substrate oxidation, and H_2O splitting, the mechanisms of which are not fully understood. Metal−peroxo and high-valent metal−oxo species are proposed to be involved as intermediates.[4−8,12,13] The formation of strong MO−H bonds provides a driving force for the latter to abstract H atoms from strong X−H bonds (X = C, N, O).[14,15] Thiolates (RS$^−$) have been shown to facilitate O_2 activation[16] via the formation of highly covalent M(III)−SR bonds[17] and to facilitate hydrogen atom transfer (HAT) reactions[14] by increasing the metal−oxo

basicity.[15] Understanding the metal ion properties that favor O−H and O−O bond formation versus cleavage should facilitate the development of catalysts tailored to promote C−H activation or H_2O splitting.

MANGANESE DIOXYGEN CHEMISTRY

In contrast to iron and copper dioxygen chemistry,[2,3,5,7,8,13,15] manganese dioxygen chemistry remains relatively unexplored,[12,18−21] and the spectroscopic properties of key superoxo and peroxo intermediates have yet to be elucidated. Establishing benchmark spectroscopic parameters will allow key enzymatic intermediates to be more readily identified, thereby providing mechanistic details that are currently unavailable. Potential Mn−dioxygen activation pathways, based in part on those established for Fe and Cu, are shown in Figure 1. These involve superoxo (**A**), hydroperoxo (**B**), and peroxo (end-on (**C**) or side-on (**D** and **H**)) intermediates as well as high-valent Mn(IV)−oxo (binuclear (**E**) or mononuclear (**F**)) and
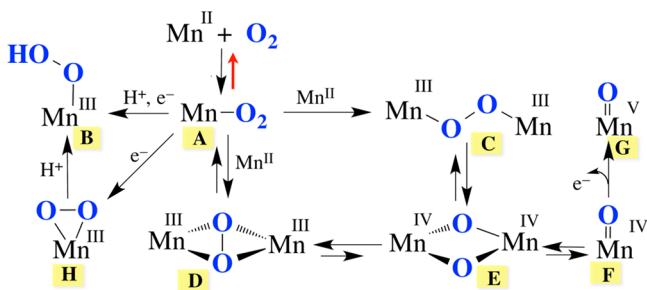
Figure 1. Proposed mechanism for dioxygen activation by Mn, based in part on established Fe and Cu pathways.

Mn(V)−oxo[22] (**G**) intermediates. A number of groups have paved the way in terms of our understanding of the properties and reactivity of Mn(IV)− and Mn(V)−oxo compounds.[22−28] High-valent Mn−oxos are typically considered to be more potent oxidants than peroxo or superoxo species and are proposed to form following heterolytic (**B** → Mn(V)≡O + H_2O) or homolytic (**C** → **E** or **D** → **E**) O−O bond cleavage (Figure 1). With Fe and Cu, peroxo O−O bond cleavage is facilitated either by protonation of the distal oxygen (**B**)[9] or bridging the peroxo between two metal ions, ideally in an η^2,η^2-side-on fashion (**D**), so as to maximize overlap with the empty σ^*(O−O) orbital.[2,7] The reverse reaction sequence (Mn(V)≡O + M−OH (M = Mn, or Ca) or Mn−O$^\bullet$ + Mn−O$^\bullet$) is proposed to be involved in the O−O bond-forming step of photosynthetic H_2O splitting, catalyzed by the oxygen evolving complex (OEC), Mn_{dang}−$CaMn_3O_4$ (Figure 2).[4,10,23,29] The
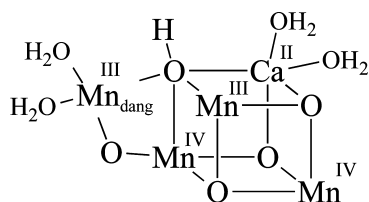

Figure 2. Structure of the OEC in its S_1 state.

dangling Mn (Mn_{dang}) has been implicated as a key player in this step. The metal ion properties that favor the forward versus reverse processes outlined in Figure 1 remain to be established.

Prior to our work,[12,20,30,31] there were no characterized examples of non-heme Mn intermediates **A**, **B**, **C**, and **D** (Figure 1), although there were a handful of examples of deprotonated versions of **B** containing an η^2-side-on peroxo (Figure 3).[18,32−35] Only one of these is derived from O_2, however.[18] Although the O−O bond in η^2-side-on Mn(III)−peroxo compounds is relatively unactivated in terms of O−O bond length, side-on peroxos have been shown to react with electrophilic aldehydes, presumably via nucleophilic attack by a "ring-opened" end-on Mn(III)−O−O$^-$ intermediate.[18,32] Con-
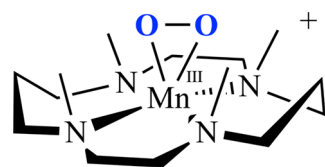

Figure 3. Representative example of a mononuclear η^2-side-on Mn−peroxo.[30]

sistent with this possibility, an end-on Mn(III)−OOH species **B** was recently shown to form upon protonation of the η^2-side-on Mn−peroxo compound shown in Figure 3, but it was not crystallographically characterized.[36]

■ LIGAND DESIGN

By making systematic changes to a metal ion's coordination sphere, one can determine how the reactivity and spectroscopic properties correlate with electronic and geometric structure of the metal ion. For the systems described herein, the ligand architecture was found to play an important role in determining both the kinetics and thermodynamics of Mn-promoted dioxygen activation (vide infra). Ligand scaffolds consisting of a thiolate (RS$^-$) and either a primary amine or N-heterocycle were assembled via a Schiff base condensation between 3-methyl-3-mercapto-2-butanone and the tetradentate amine backbones depicted in Figure 4. A thiolate was incorporated
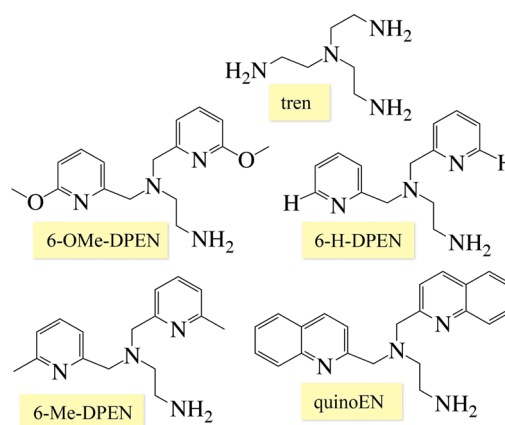

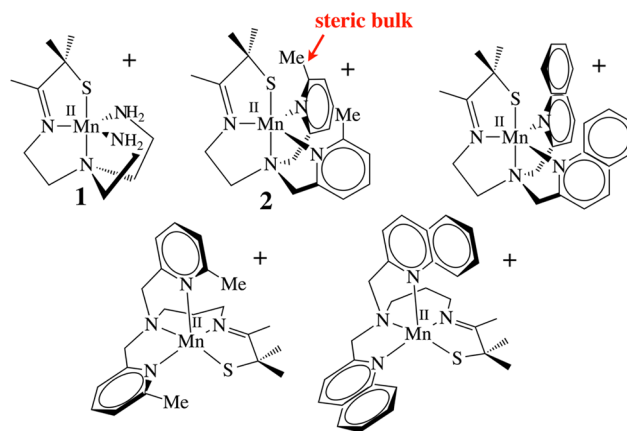**Figure 4.** Tetradentate amine ligand backbones used to construct reactive Mn(II) complexes.

Figure 5. Series of thiolate-ligated Mn(II) complexes shown to react with O_2.

(Figure 5) in order to promote O_2 binding and facilitate the observation of metastable dioxygen intermediates.[12] We have shown that the RS → M charge transfer (CT) bands of M−thiolate complexes provide a convenient spectroscopic handle for monitoring the formation of intermediates (e.g., [Fe^{III}(S^{Me2}N$_4$(tren))(OOH)]$^+$),[12,17,37−39] and the reduction of

small molecules (e.g., O_2, $O_2^{-\bullet}$, NO_2^-, and NO).[12,37,38,40] Upon oxidation, the metal-centered orbitals drop in energy closer to the sulfur orbitals of π symmetry, causing the RS → M CT band to shift from the UV to the visible region.[17] This also increases the M−SR bond covalency, providing a driving force for RS−M(III)−$O_2^{\bullet-}$ formation from RS−M(II) + O_2 and lowering the activation barrier to O_2 binding.[16] We found that with Mn, the thiolate's contributions to the electronic spectral properties turn out to be especially important because in contrast to Cu and Fe, the peroxo → M CT band falls in the UV as opposed to the visible region of the spectrum.[2,5,30] N-heterocycles were incorporated into our ligand design because they are easily derivatized, allowing us to readily tune the electronic and steric properties of the corresponding manganese complexes (Figure 5). Substituents at the 6-position were varied from R = H, Me, or OMe to a fused phenyl ring (i.e., quinoline), and the number of methylene units $(CH_2)_n$ connecting the tertiary amine to the imine was varied from n = 2 to 3. Subtle differences in the ligand scaffold were found to significantly affect the O_2 reactivity[41] and our ability to observe metastable intermediates, illustrating the importance of judicious ligand design and modification.

DIOXYGEN ACTIVATION BY SYNTHETIC MN(II) COMPLEXES

At ambient temperatures, all of the Mn(II) complexes pictured in Figure 5 were shown to react with O_2 to form relatively stable binuclear Mn(III) complexes containing a single oxo atom bridge in high yields (96−98%).[12,41] At low temperatures, metastable dioxygen intermediates are observed,[12,19] but only if steric bulk is incorporated into the ligand backbone. The N-heterocycle substituent was found to dramatically influence both the relative and overall stabilities of Mn−dioxygen intermediates. With primary amines (tren, 1)[41] or with an R = H substituent at the 6-position of the pyridine (6-H-DPEN, Figure 4), no dioxygen intermediates are observed, even at temperatures as low as −78 °C. With a Me substituent at the 6-position, on the other hand, the reduced five-coordinate complex $[Mn^{II}(S^{Me2}N_4(6\text{-MeDPEN}))]^+$ (2) was shown to react with 1 equiv of O_2 at low T (Figure 6) to irreversibly form the dioxygen intermediate $[Mn(S^{Me2}N_4(6\text{-MeDPEN}))(O_2)]^+$ (3), observable by stopped-flow (λ_{max} = 515 nm, $k_1(-10\ °C)$ =

3780 $M^{-1}\ s^{-1}$, $\Delta H_1^{\ddagger}$ = 26.4 kJ/mol, $\Delta S_1^{\ddagger}$ = −75.6 J mol^{-1} K^{-1}),[12] which then more slowly converts to the metastable green intermediate $\{[Mn^{III}(S^{Me2}N_4(6\text{-MeDPEN})]_2(\mu\text{-}O_2)\}^{2+}$ (4) (λ_{max} = 640(830) nm, $k_2(-10\ °C)$ = 417 $M^{-1}\ s^{-1}$, $\Delta H_2^{\ddagger}$ = 47.1 kJ/mol, $\Delta S_2^{\ddagger}$ = −15 J $mol^{-1}\ K^{-1}$). Binding of dioxygen to 2 is relatively slow compared with binding to Cu(I) complexes.[3,7] Metastable 4 slowly converts (∼4 h at −40 °C) to the purple mono-oxo-bridged product $\{[Mn^{III}(S^{Me2}N_4(6\text{-MeDPEN})]_2(\mu\text{-}O)\}^{2+}$ (5) (λ_{max} = 560 nm) in high yields (97−99%). The oxo atom in 5 (Figure 6) is derived from O_2, as shown by $^{18}O_2$ labeling studies. This would be consistent with O−O bond cleavage occurring along the reaction pathway.

CHARACTERIZATION OF A MN−PEROXO INTERMEDIATE DERIVED FROM O_2

Intermediate 4 (Figure 6) was found to release H_2O_2 upon protonation and to display isotopically sensitive stretches in the resonance Raman (rR) spectrum ($\nu_{O-O}(\Delta^{18}O)$ = 819(47) cm^{-1}, $\nu_{Mn-O}(\Delta^{18}O)$ = 611(25) cm^{-1}; Figure 7), consistent with
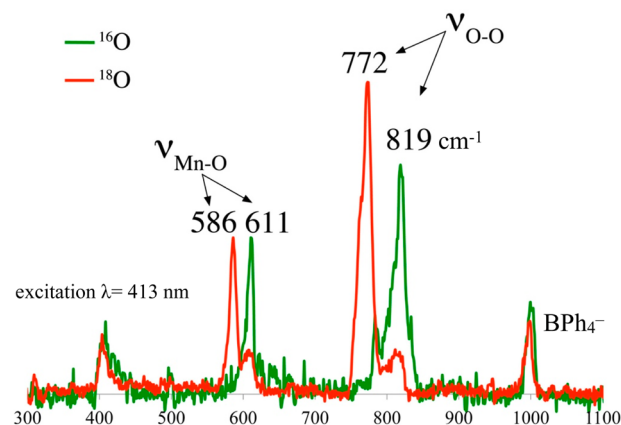
Figure 7. Resonance Raman spectrum of peroxo intermediate 4 (^{16}O (green) vs ^{18}O (red)).

a peroxo.[12] This assignment was ultimately verified by X-ray crystallography, which showed two Mn^{3+} ions bridged by a peroxo in an end-on *trans-μ*-1,2 fashion (Figure 8).[12] The two
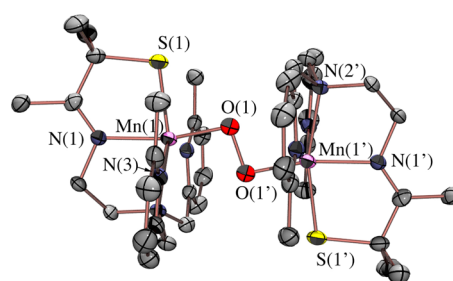
Figure 8. ORTEP diagram of O_2-derived peroxo intermediate 4.

electrons required to convert O_2 to O_2^{2-} are derived from the two Mn^{2+} ions required to form 4. Overall, the kinetics of peroxo 4 formation show a second-order dependence on Mn(II) and a first-order dependence on O_2.[12] Consistent with two-electron reduction of O_2, the O−O bond in 4 (1.452(5) Å) is significantly longer than that in O=O (1.21 Å) and close to that in reduced peroxide $O-O^{2-}$ (1.49 Å). The coexistence of a thiolate (a reductant) and a peroxide (an oxidant) in the same
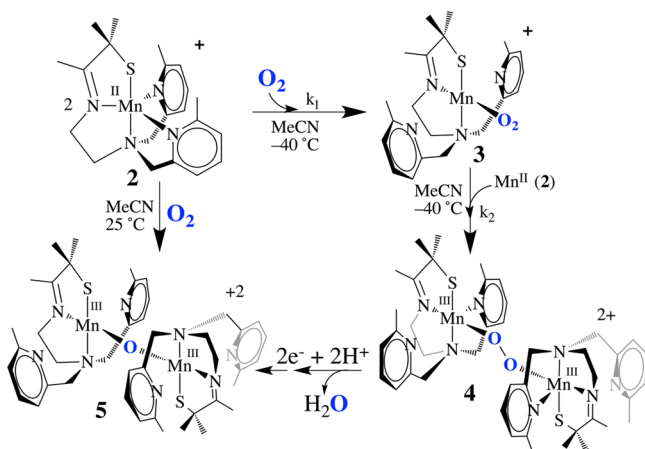

Figure 6. Reaction of five-coordinate 2 with O_2 to afford mono-oxo-bridged 5 via metastable Mn−O_2 intermediate 3 and Mn−peroxo intermediate 4.

molecule is quite remarkable and perhaps suggests that the bridging peroxo is not a particularly strong oxidant. Compared with the peroxo O−O bonds of the more predominant mononuclear η^2-side-on Mn(III)−peroxo complexes (Figure 3), with lengths in the range 1.403(4)−1.428(7) Å,[32−35] that of **4** is noticeably longer. It is, however, comparable to those of lower-resolution *cis*-μ-1,2-peroxo-bridged Mn(IV) dimer (1.46(3) Å),[21] and *cis*-μ-1,2-peroxo-bridged trinuclear (1.6(1) Å)[42] structures, indicating that the bridging mode is responsible for the longer O−O bond. The isotopically sensitive ν_{O-O} stretching frequency of **4** is the lowest reported for a Mn−peroxo,[18,34] consistent with its long O−O bond length and unique bridging mode.

Peroxo-bridged **4** was not only the first well-defined example of a *trans*-μ-1,2-end-on Mn(III)−peroxo but also the first Mn−peroxo to be characterized by resonance Raman spectroscopy.[12] The electronic absorption spectrum of **4** displays two bands, one at λ_{max} = 387(1200) nm and the other at λ_{max} = 640(830) nm. Resonance enhancement of the isotopically sensitive ν_{O-O} and ν_{Mn-O} stretches in Figure 7 is observed only with laser frequencies near the UV, leading us to conclude that the higher-energy band at 387 nm rather than the lower-energy band at 640 nm corresponds to the $\pi_v^*(O-O) \rightarrow$ Mn CT band. This is in contrast to Fe−peroxo species, which have intense peroxo-to-metal CT bands in the visible region (500−700 nm),[5,8,37] and may be one of the reasons there are no other reported rR-characterized Mn−peroxo species, except for recently reported Mn(III)−OOH.[36]

■ OBSERVED CORRELATION BETWEEN STRUCTURE AND SPECTROSCOPIC PROPERTIES OF MN−PEROXO COMPOUNDS

An unusual structural feature of peroxo-bridged **4**, which turns out to play a key role in our ability to observe this metastable dioxygen intermediate, is the weakly coordinated pyridines (Figure 9). The Mn···N^{py} distances in **4** (2.410(3) and
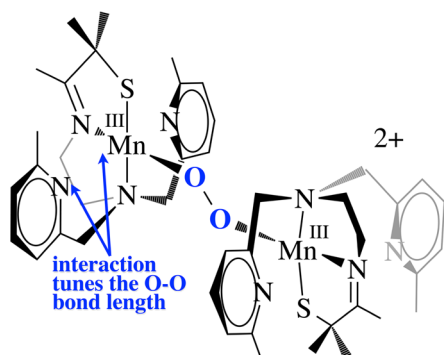

Figure 9. The N-heterocycle influences the peroxo O−O bond length in all of the peroxo compounds examined in this series, including **4**, even though they are well outside the typical bonding range.

2.492(3) Å) are well outside the typical range (2.17−2.25 Å) and significantly longer than the sum of their covalent radii (2.105 Å). Similarly long distances are observed in mono-oxo-bridged **5**. Space-filling models indicate that steric interactions between the 6-methylpyridine substituent and the *gem*-dimethyl group adjacent to the sulfur are likely responsible for the long Mn···N^{py} distances. Although Jahn−Teller-like distortions possibly contribute to the elongation of these bonds, the Mn−N^{py} bonds in the less sterically congested 6-H-DPEN

(Figure 4)-ligated Mn(III) oxo-bridged species are significantly shorter (2.223(5) and 2.243(5) Å), indicating that steric interactions play an important role. Peroxo **4** can therefore technically be described as a coordinatively unsaturated molecule. We observe similarly long Mn···N^{py,quino} "bonds" (2.349(7)−2.522(8) Å) in the series of structurally characterized metastable alkylperoxo Mn(III)−OOR (R = ^{t}Bu, CMe$_2$Ph) compounds **6−11** (Figure 10), the first reported examples of this type.[30,31] Not only is it rare for one to be able to crystallize a first-row transition-metal peroxo, but to do so with a series of structurally related molecules (selected examples are shown in Figure 11) is *extraordinarily rare, if not unprecedented*. Thus, we were provided with an opportunity to look for correlations between key properties that are likely to influence O−O bond cleavage and formation. Strong correlations between structural, spectroscopic, and kinetic parameters were in fact observed.[30] For example, the peroxo O−O bond length was shown to be inversely correlated with the Mn···N^{py,quino} distance (Figure 12). The O−O bond was found to elongate as the N-heterocycle moves closer to the Mn ion. Parameters for O$_2$-derived peroxo **4** also fall on this line (red triangle in Figure 12). An extrapolation of this line to include a Mn−N^{py} distance of 2.23 or 2.31 Å would predict that the peroxo compounds containing the unsubstituted pyridine (6-H-DPEN) and primary amine (tren) ligands (Figure 4) would have O−O bond lengths of 1.55 and 1.51 Å, respectively, which would be significantly longer than the O−O bond of free peroxide O$_2^{2-}$ (1.49 Å). This extrapolation assumes that, as observed with the other peroxo/oxo compounds described above, the (unobserved) peroxo intermediate and the final mono-oxo-bridged Mn(III)−oxo possess similar Mn−N^{py} distances.[41] This explains why we were unable to observe peroxo intermediates with the less sterically encumbered ligands. Extrapolation of this line to ≥2.8 Å (i.e., removal of the pyridines) would result in a significantly shorter O−O bond (≤1.32 Å). The "dangling" pyridines provide a potential H$^+$ relay site that could be used either to facilitate heterolytic O−O bond cleavage or deprotonation of a coordinated H$_2$O.

The data described above demonstrate that the N-heterocycle has a profound effect on the degree of O−O bond activation observed in our peroxo complexes, even when they lie well outside the expected bonding range. A density functional theory (DFT)-generated bonding picture[30] for the alkylperoxo Mn(III)−OO^{t}Bu complex **9** (Figure 11) shows that the Mn···N^{py} interaction modulates the π overlap between the filled peroxo $\pi_v^*(O-O)$ orbital and the Mn d$_{xz}$ orbital by altering the metal ion Lewis acidity: the Mulliken charge density was shown to increase (from +0.42 to +0.50) as the Mn···N^{py,quino} distance increases.[30] As the metal ion Lewis acidity increases, the d manifold drops in energy toward the peroxo oxygen orbitals, thereby increasing σ(Mn−O^{peroxo}) and π(Mn−O^{peroxo}) bonding interactions. An increased π interaction shifts electron density out of the filled antibonding peroxo $\pi_v^*(O-O)$ orbital into the Mn−O^{peroxo} bonding region, resulting in a shorter, stronger peroxo O−O bond and ultimately an isolable Mn−peroxo.[30] If the d orbitals drop in energy toward the peroxo orbitals, this would predict that the energy of the peroxo → M CT band should decrease as the Mn···N^{py,quino} separation increases and the O−O bond length decreases. This is in fact what we observe. The electronic absorption spectra of the intense-blue Mn−peroxo compounds **6−11** described above display two bands (as shown for **8** in Figure 13), one of which tracks with the O−O bond length. As
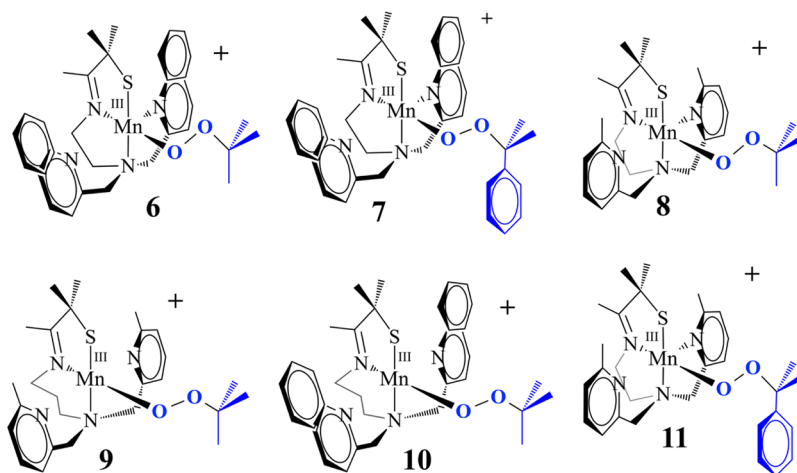
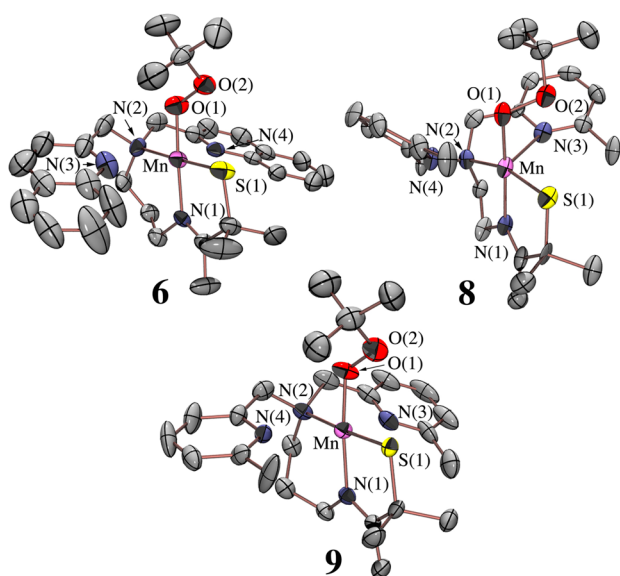**Figure 10.** Series of structurally related metastable Mn(III)−OOR complexes.

Figure 11. ORTEP diagrams of crystallized metastable Mn(III)−OOR complexes (representative examples).
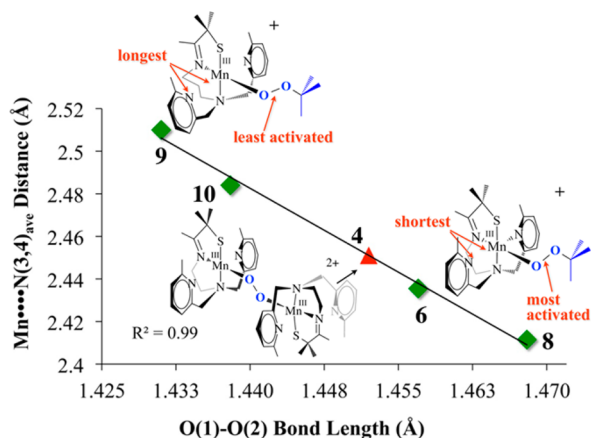

Figure 12. Correlation between the Mn···N^{py,quino} distance and the peroxo O−O bond length in Mn(III)−OOR compounds and O_2-derived **4**.

Figure 13. Electronic absorption spectrum of metastable Mn(III)−OOR complex **8** (R = ^{t}Bu).
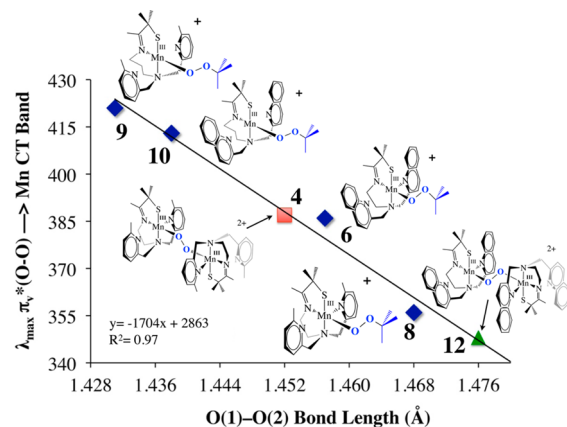
Figure 14. Correlation between the peroxo → Mn(III) CT band energy and the peroxo O−O bond length.

decreases as the O−O bond length decreases. Parameters for O_2-derived peroxo **4** also fall on this line (red square in Figure 14). The energy difference (∼70 nm) between the CT bands for the complexes with the shortest and longest peroxo O−O bonds shows that these distances are spectroscopically distinguishable. We can therefore use this spectroscopic parameter to estimate the O−O bond length, and thus the degree of O−O bond activation, in related Mn(III)−peroxo intermediates for which there is no crystal structure. This would

shown in Figure 14, the energy of the band in the near-UV region of the spectrum (e.g., λ_{max} = 356 nm in Figure 13)
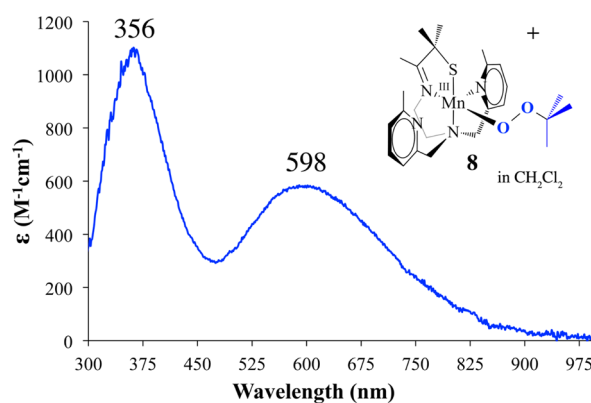
of course require that the ligand environment be roughly the same. For example, although we have not been able to grow high-quality crystals of an O_2-derived quinoline−Mn−peroxo intermediate (green triangle in Figure 14), we can estimate its O−O bond length using the experimentally determined peroxo → Mn CT band energy (λ_{max} = 348 nm) and the linear fit to the data. The long O−O bond estimated in this manner (1.476 Å) is consistent with the significantly shorter lifetime of the quinoline peroxo ($t_{1/2}$(233 K) = 47 s; k = 0.0149 s^{-1}) relative to **4** ($t_{1/2}$(233 K) ≈ 45 min).[19]

In collaboration with the DeBeer group, Kβ X-ray emission spectroscopy (XES) was pursued in order to examine factors favoring O−O bond activation in O_2-derived **4** and to provide a molecular orbital (MO) picture of the bonding.[20] X-ray absorption spectroscopy (XAS) involves the promotion of a metal ion 1s electron into either discrete orbitals (the pre-edge) or the continuum. XES involves the relaxation of a metal 3p electron (the K$\beta_{1,3}$ and Kβ' mainline region) or a ligand-based 2s or 2p electron (the Kβ'' and K$\beta_{2,5}$ valence-to-core (VtC) region) into the 1s hole. This method has been used successfully to quantify N_2 activation in Fe−N_2 complexes.[43] We are interested in obtaining benchmark parameters and looking for correlations between key emission features and O−O bond lengths in Mn−peroxo compounds. As shown in Figure 15, fits to the XES spectrum of peroxo-bridged **4** (black)
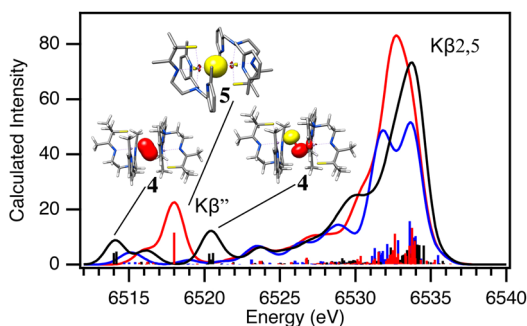

Figure 15. XES spectrum of O_2-derived peroxo intermediate **4** (black) vs those of oxo-bridged **5** (red) and Mn(II) **2** (blue).

show two features in the region 6514−6521 eV[20] that are not present in the spectrum of the Mn(II) precursor **2** (blue) and lie above and below that involving the O 2s orbital of oxo-bridged **5** (red). These features correspond to emission from the peroxo σ_{2s}(O−O) and σ_{2s}^*(O−O) orbitals, the separation of which reflects the peroxo O−O bond strength. DFT-calculated fits to the experimental XES data were used to generate a bonding picture of **4** (Figure 16),[20] which shows that the
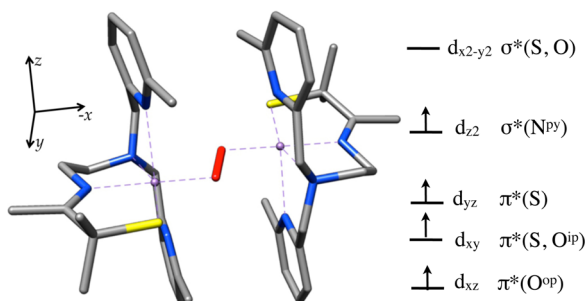

Figure 16. HOMO/LUMO region of the DFT-calculated MO diagram of peroxo-bridged **4**.

thiolate and peroxo ligands dominate the ligand field, resulting in an empty $d_{x^2-y^2}$ σ^* orbital and leaving the pyridine nitrogens pointing toward the half-occupied d_{z^2} orbital, thereby providing a mechanism for modulating the metal ion Lewis acidity. Pseudo-σ overlap between the thiolate sulfur, half-occupied Mn d_{xy}, and peroxo π_{ip}^* orbitals (Figure 17) provides an additional
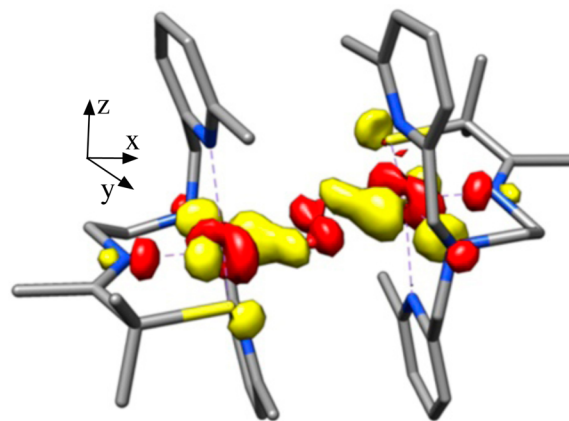

Figure 17. DFT-calculated MO involving overlap between the peroxo π_{ip}^*, Mn d_{xy}, and thiolate sulfur orbitals of peroxo-bridged **4**.

mechanism for elongating the peroxo O−O bond.[20] On the basis of the above structural, theoretical, and spectroscopic data, it is tempting to suggest that the eventual O−O bond cleavage that occurs with these metastable peroxos results from vibrational compression along the Mn−N^{py,quino} vectors. The thiolate also plays an important role in promoting O−O bond cleavage via a "push" mechanism[20] much like that proposed to be involved in the ^{cys}S-promoted O−O bond cleavage step of P450.

CORRELATION BETWEEN REACTIVITY AND STRUCTURAL AND SPECTROSCOPIC PROPERTIES

Rate-limiting peroxo O−O bond cleavage constitutes the mechanism of decay of our metastable Mn(III)−OOR compounds (Figure 10), as shown by the strong correlation between the enthalpy of activation ($\Delta H^{\ddagger}$) and the peroxo O−O bond length (Figure 18).[30] The Mn···N^{py,quino} interaction plays an integral role. The value of $\Delta H^{\ddagger}$ progressively decreases (from 15.9 to 10.4 kcal/mol) as the average Mn···N^{py,quino} distance decreases (from 2.51 to 2.41 Å).[30] The exclusive formation of acetophenone (72% yield) as opposed to cumenol
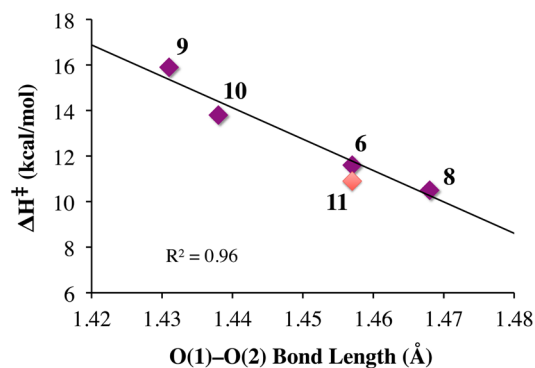

Figure 18. Correlation between $\Delta H^{\ddagger}$ and the peroxo O−O bond length of Mn(III)−OOR (R = ^{t}Bu (purple), Cm (red)) complexes.

upon warming cumenyl (Cm) peroxo derivatives **7** and **11** (Figure 10) provides evidence for homolytic as opposed to heterolytic O−O bond cleavage.[31] The rate constants were found to be insensitive to the presence of electrophilic or nucleophilic organic substrates. The formation of Et_2PO^tBu (24%) + Et_3PO (31%) upon warming of Mn(III)−OO^tBu derivatives **6** and **8−10** in the presence of PEt_3 is also consistent with homolytic as opposed to heterolytic O−O bond cleavage.[31] The formation of Et_3PO implies that a Mn(IV)−oxo intermediate is involved.

In order to convert dioxygen-derived peroxo-bridged **4** to mono-oxo-bridged **5**, two electrons and at least one or likely two protons are required (Figure 6). The fate of the second O atom and the source of additional reducing equivalents ($2e^-$ + $2H^+$) remain to be determined. We suspect that a high-valent Mn−oxo intermediate, formed during the course of the reaction, abstracts H atoms from the solvent. However, to date we have only circumstantial evidence[19,44] to support this. The reproducibly observed high yield of **5** rules out Mn^{2+} or sacrificial ligand as a source of H atoms or electrons, respectively. External substrates (PPh_3, 2,4-$^tBu_2$-PhOH) are oxidized by Mn(II) **2** + O_2 and serve as an electron (or e^- + H^+) source.[19] However, the rate of peroxo **4** decay is not affected by added external substrates, indicating that the reactive species responsible for the observed oxidation chemistry forms following rate-limiting O−O bond cleavage, much like the Mn(III)−OOR compounds described above.[19] This suggests that the peroxo itself is not very reactive. As revealed by space-filling models, this may in part be due to the inaccessibility of the peroxo, which is flanked by four π-stacked aromatic rings.[12] With PPh_3, 15 turnovers are achieved with almost no degradation of the catalyst. With 2,4-$^tBu_2$-PhOH, mono-oxo-bridged **5** forms in addition to the oxidized biphenol product (52% yield).[19] The second oxygen is most likely lost as H_2O via the condensation of two Mn(III)−OH intermediates. Isotopically labeled ^{18}O is incorporated into the oxo bridge of **5** when $H_2{}^{18}O$ is added to **2** + $^{16}O_2$, also supporting the involvement of a Mn(IV)=O intermediate. No label is incorporated when $H_2{}^{18}O$ is added to **5** alone as a control.[19] The less sterically encumbered, more electron-rich 6-OMe-DPEN-ligated derivative of **2**, shown in Figure 19, converts 1,4-
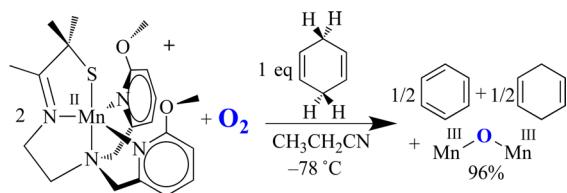

Figure 19. Reaction between O_2 and the more electron-donating 6-OMe-DPEN-ligated Mn(II) complex in the presence of CHD affords benzene.

cyclohexadiene (CHD) to benzene.[19] In the absence of an external H atom donor, it is possible that MeCN solvent, or some impurity therein, serves as a H atom (e^- + H^+) source. Evidence to support this possibility is provided by results showing that deuterium from CD_3CN is incorporated into the bis(μ-OD)-bridged product formed upon the addition of O_2 (or PhIO) to $[Fe^{II}(O^{Me2}N_4(6\text{-MeDPEN}))]^+$ (**12**) (Figure 20).[44] On the basis of the MeCN C−H bond dissociation free energy (BDFE) of 97 kcal/mol,[14] this would require a potent oxidant. With a coordinated thiolate (or possibly an

alkoxide), one would expect a Mn(IV)=O species to be highly reactive, much like the $RS^{\bullet+}$−Fe(IV)=O of P450. In fact, we found that even the reduced, protonated, thiolate-ligated Mn(III)−OH complex $[Mn^{III}(S^{Me2}N_4(tren))(OH)]^+$ (**13**) can abstract H atoms, albeit from weak X−H bonds such as that in TEMPOH (O−H BDFE = 66.5 kcal/mol; Figure 21).[45] This is despite the fact that **13** is an extremely mild oxidant ($E_{1/2}$ = −300 mV vs $Cp_2Fe^{+/0}$ in MeCN). The reactive species **13** can be aerobically regenerated in H_2O, and at least 10 turnovers can be achieved with almost no degradation of the "catalyst".[45] Hydroxo-bound **13** is the only water-soluble Mn(III)−OH complex shown to promote HAT. Consistent with this reactivity, **13** displays proton-coupled electron transfer (PCET) in H_2O, and from the linear correlation between its redox potential and the pH we were able to calculate an aqueous O−H BDFE of 74.0(5) kcal/mol for the product $[Mn^{II}(S^{Me2}N_4(tren))(H_2O)]^+$ (**14**). From this we could estimate the O−H BDFE for **14** in MeCN (70.1 kcal/mol) and calculate its pK_a as 21.2.[45] The thiolate was shown to increase the basicity of the hydroxo ligand, offsetting the low potential, thereby facilitating H atom abstraction.[45] This work demonstrates that the O−H BDFE of H_2O (122.7 kcal/mol) is decreased considerably (by 48.7 kcal/mol) upon binding to Mn^{2+},[45] an observation relevant to the mechanism of photosynthetic H_2O splitting.

■ CONCLUDING REMARKS

Dioxygen formation and its controlled activation for incorporation into organic molecules drive the chemistry of life as we know it. Key steps in these reactions involve transition-metal-promoted cleavage and/or formation of O−H and O−O bonds via metal−oxo and −peroxo intermediates, but we are far from understanding the mechanistic details, especially with Mn. By systematically altering the metal ion coordination sphere, we have shown that subtle differences in ligand architecture can significantly affect the relative stability of Mn−dioxygen intermediates and tune peroxo O−O bond lengths. By crystallizing an entire series of metastable Mn(III)−peroxo compounds with varying degrees of O−O bond activation, we have demonstrated that there are distinct correlations between spectroscopic, structural, and reactivity properties. Weakly coordinated N-heterocycles have been shown to be responsible for our ability to observe these peroxos and to cause the O−O bond length to vary as a function of Mn···$N^{py,quino}$ distance by modulating the π overlap between the filled peroxo π_v^*(O−O) and Mn d_{xz} orbitals. We have shown that there is a strong correlation between the peroxo → Mn CT band and the peroxo O−O bond length, and the energy difference between the CT bands for the complexes with the shortest and longest O−O bonds shows that these distances are spectroscopically distinguishable, indicating that we can use this spectroscopic parameter to predict an estimated O−O bond length, and thus the degree of O−O bond activation, in intermediates for which there is no crystal structure, as long as the ligand environment is roughly the same.

Of the proposed intermediates outlined in Figure 1, two have yet to be characterized: a binuclear bridging η^2,η^2-side-on Mn(III)−peroxo (**D**) and a well-defined Mn(III)−superoxo (**A**). We have shown that several metastable intermediates can be observed in the reaction between O_2 and our coordinatively unsaturated Mn(II) complexes (Figure 5), including the first crystallographically characterized example of a binuclear *trans-μ-1,2-peroxo-bridged Mn(III) intermediate (**C**), a Mn−O_2
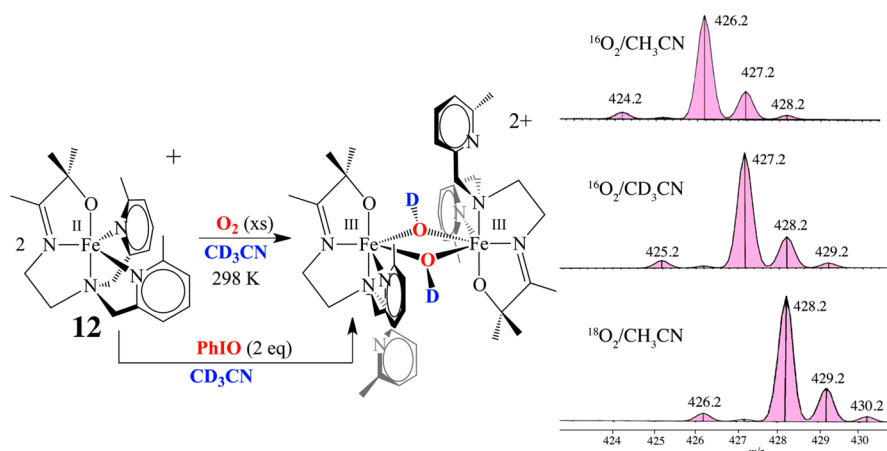
Figure 20. Deuterium incorporation into the product of the reaction between O_2 (or PhIO) and an alkoxide-ligated Fe(II) complex in CD_3CN.
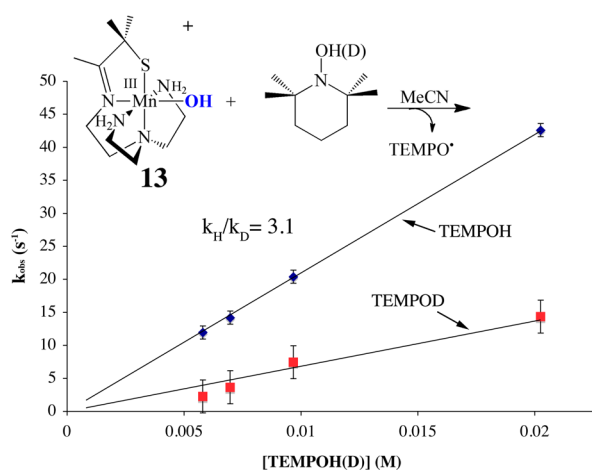

Figure 21. Deuterium isotope effect demonstrating that reduced protonated Mn(III)−OH abstracts a hydrogen atom from TEMPOH-(D).

intermediate (**A**) (Figure 1), and a third intermediate (**E** or **F**) implicated via indirect (reactivity) evidence. Rate-limiting O−O bond cleavage affords a reactive species capable of abstracting H atoms from 2,4-$^tBu_2$-PhOH or 1,4-cyclohexadiene depending on the supporting ligand substituents. *The observation of more than one intermediate is exceedingly rare* in first-row transition-metal O_2 chemistry outside of a protein environment.[2,3,6,7] The instability of our Mn−O_2 intermediate **3** did not allow us to determine whether it is best described as a Mn(III)−$O_2^{•-}$ (superoxo) or Mn(II)−O_2 species. Obtaining a well-defined Mn−superoxo would allow one to determine whether such a species is capable of abstracting H atoms and/or reductively eliminating O_2 upon oxidation. We have shown that O_2 binds *irreversibly* to our Mn(II) complex, which is in contrast to its behavior with Fe and Cu.[3,12] It is possible that the thiolate ligand contributes to this irreversibility. However, as illustrated by OEC-promoted (Figure 1) biological O_2 evolution,[4] one would expect a higher oxidation state to be required in order for Mn to promote reductive elimination of O_2[46] because the Mn(II) d orbitals lie higher in energy than those of Cu(I) or Fe(II) relative to oxygen.

The first steps of photosynthetic H_2O splitting ($S_0 \rightarrow S_4$)[4,10,29] involve the endothermic cleavage of strong O−H bonds (122.7 kcal/mol) via PCET.[14] We have shown that the O−H BDFE of H_2O decreases considerably upon binding to

Mn^{2+}.[45] Mechanistic details about the steps that follow, involving O−O bond formation and reductive elimination of O_2 ($S_4 \rightarrow S_0$), are unavailable.[4,10,22,29] An unobserved Mn−peroxo species (S_2^*),[47] resembling our structurally characterized binuclear *trans*-μ-1,2-peroxo-bridged Mn complex **4**, has been proposed to be involved as a key intermediate. However, the longer O−O bonds of binuclear Mn(III) peroxo-bridged **4** and related binuclear Mn(IV) peroxo-bridged species[21] relative to those of mononuclear Mn(III)−peroxos indicate that dioxygen is more effectively activated when bridged between two Mn ions regardless of the oxidation state. This suggests that such a species is unlikely to be involved as an intermediate in photosynthetic O_2 evolution, which would be consistent with the proposed involvement of the OEC Mn_{dang} and Ca^{2+} ions (Figure 2).[4,10,22,29]

■ **AUTHOR INFORMATION**

Corresponding Author

*E-mail: kovacs@chem.washington.edu.

Notes

The authors declare no competing financial interest.

Biography

Julie A. Kovacs is a Professor of Chemistry at the University of Washington in Seattle. She received her B.S. degree from Michigan State University (1981) and her Ph.D. from Harvard University (1986) and did her postdoctoral work at UC Berkeley. Her research focuses on characterizing metastable intermediates formed during transition-metal-promoted dioxygen activation and determining how thiolate ligands influence their properties.

■ **ACKNOWLEDGMENTS**

■ **REFERENCES**

(1) Cotruvo, J. A., Jr.; Stich, T. A.; Britt, R. S.; Stubbe, J. Mechanism of Assembly of the Dimanganese-Tyrosyl Radical Cofactor of Class Ib Ribonucleotide Reductase: Enzymatic Generation of Superoxide Is Required for Tyrosine Oxidation via a Mn(III)Mn(IV) Intermediate. *J. Am. Chem. Soc.* **2013**, *135*, 4027−4039.

(2) Solomon, E. I.; Heppner, D. E.; Johnston, E. M.; Ginsbach, J. W.; Cirera, J.; Qayyum, M.; Kieber-Emmons, M. T.; Kjaergaard, C. H.; Hadt, R. G.; Tian, L. Copper Active Sites in Biology. *Chem. Rev.* **2014**, *114*, 3659−3853.

(3) Lee, J. Y.; Karlin, K. D. Elaboration of copper−oxygen mediated C−H activation chemistry in consideration of future fuel and feedstock generation. *Curr. Opin. Chem. Biol.* **2015**, *25*, 184−193.

(4) Yano, J.; Yachandra, V. K. Mn4Ca Cluster in Photosynthesis: Where and How Water is Oxidized to Dioxygen. *Chem. Rev.* **2014**, *114*, 4175−4205.

(5) Tinberg, C. E.; Lippard, S. J. Dioxygen Activation in Soluble Methane Monooxygenase. *Acc. Chem. Res.* **2011**, *44*, 280−288.

(6) Kovaleva, E. G.; Neibergall, M. B.; Chakrabarty, S.; Lipscomb, J. D. Finding Intermediates in the O$_2$ Activation Pathways of Non-Heme Iron Oxygenases. *Acc. Chem. Res.* **2007**, *40*, 475−483.

(7) Lewis, E. A.; Tolman, W. B. Reactivity of dioxygen-copper systems. *Chem. Rev.* **2004**, *104*, 1047−1076.

(8) Costas, M.; Mehn, M. P.; Jensen, M. P.; Que, L. J. Dioxygen Activation at Mononuclear Nonheme Iron Active Sites: Enzymes, Models, and Intermediates. *Chem. Rev.* **2004**, *104*, 939−986.

(9) Kovacs, J. A. How Iron Activates O$_2$. *Science* **2003**, *299*, 1024−1025.

(10) Suga, M.; Akita, F.; Hirata, K.; Ueno, G.; Murakami, H.; Nakajima, Y.; Shimizu, T.; Yamashita, K.; Yamamoto, M.; Ago, H.; Shen, J.-R. Native structure of photosystem II at 1.95 Å resolution viewed by femtosecond X-ray pulses. *Nature* **2015**, *517*, 99−103.

(11) Young, K. J.; Brennan, B. J.; Tagore, R.; Brudvig, G. W. Photosynthetic Water Oxidation: Insights from Manganese Model Chemistry. *Acc. Chem. Res.* **2015**, *48*, 567−574.

(12) Coggins, M. K.; Sun, X.; Kwak, Y.; Solomon, E. I.; Rybak-Akimova, E.; Kovacs, J. A. Characterization of Metastable Intermediates Formed in the Reaction Between a Mn(II) Complex and Dioxygen, Including a Crystallographic Structure of a Binuclear Mn(III)-Peroxo Species. *J. Am. Chem. Soc.* **2013**, *135*, 5631−5640.

(13) Solomon, E. I.; Wong, S. D.; Liu, L. V.; Decker, A.; Chow, M. S. Peroxo and oxo intermediates in mononuclear non-heme iron enzymes and related active sites. *Curr. Opin. Chem. Biol.* **2009**, *13*, 99−113.

(14) Warren, J. J.; Tronic, T. A.; Mayer, J. M. Thermochemistry of Proton-Coupled Electron Transfer Reagents and its Implications. *Chem. Rev.* **2010**, *110*, 6961−7001.

(15) Green, M. T. C−H bond activation in heme proteins: the role of thiolate ligation in cytochrome P450. *Curr. Opin. Chem. Biol.* **2009**, *13*, 84−88.

(16) Brown, C. D.; Neidig, M. L.; Neibergall, M. B.; Lipscomb, J. D.; Solomon, E. I. VTVH-MCD and DFT Studies of Thiolate Bonding to {FeNO}^{7}/{FeO$_2$}^{8} Complexes of Isopenicillin N Synthase: Substrate Determination of Oxidase versus Oxygenase Activity in Nonheme Fe Enzymes. *J. Am. Chem. Soc.* **2007**, *129*, 7427−7438.

(17) Kovacs, J. A.; Brines, L. M. Understanding how the thiolate sulfur contributes to the function of the non-heme iron enzyme superoxide reductase. *Acc. Chem. Res.* **2007**, *40*, 501−509.

(18) Shook, R. L.; Gunderson, W. A.; Greaves, J.; Ziller, J. W.; Hendrich, M. P.; Borovik, A. S. A Monomeric MnIII-Peroxo Complex Derived Directly from Dioxygen. *J. Am. Chem. Soc.* **2008**, *130*, 8888−8889.

(19) Johansen, A.; Rees, J. A.; Hayes, E.; Coggins, M. K.; Stoll, S.; Rybak-Akimova, E.; DeBeer, S.; Kovacs, J. A. Tuning the Ligand Environment To Favor Mn(II)-Promoted Dioxygen Activation and O−O Bond Cleavage. Manuscript in preparation.

(20) Rees, J. A.; Martin-Diaconescu, V.; Kovacs, J. A.; DeBeer, S. X-ray Absorption and Emission Study of Dioxygen Activation by a Small-Molecule Manganese Complex. *Inorg. Chem.* **2015**, *54*, 6410−6422.

(21) Bossek, U.; Weyhermüller, T.; Wieghardt, K.; Nuber, B.; Weiss, J. [L$_2$Mn$_2$(μ-O)$_2$(μ-O$_2$)](ClO$_4$): The First Binuclear(μ-Peroxo)-dimanganese(IV) Complex (L = 1,4,7Trimethyl-1,4,7triazacyclono-nane). A Model for the S$_4$-S$_0$ Transformation in the Oxygen Evolving Complex in Photosynthesis. *J. Am. Chem. Soc.* **1990**, *112*, 6387−6388.

(22) Gupta, R.; Taguchi, T.; Lassalle-Kaiser, B.; Bominaar, E. L.; Yano, J.; Hendrich, M. P.; Borovik, A. S. High-spin Mn−oxo complexes and their relevance to the oxygen-evolving complex within photosystem II. *Proc. Natl. Acad. Sci. U. S. A.* **2015**, *112*, 5319−5324.

(23) Mukherjee, S.; Stull, J. A.; Yano, J.; Stamatatos, T. C.; Pringouri, K.; Stich, T. A.; Abboud, K. A.; Britt, R. D.; Yachandra, V. K.; Christou, G. Synthetic model of the asymmetric [Mn$_3$CaO$_4$] cubane core of the oxygen-evolving complex of photosystem II. *Proc. Natl. Acad. Sci. U. S. A.* **2012**, *109*, 2257−2262.

(24) Prokop, K. A.; Goldberg, D. P. Generation of an Isolable, Monomeric Manganese(V)−Oxo Complex from O$_2$ and Visible Light. *J. Am. Chem. Soc.* **2012**, *134*, 8014−8017.

(25) Jin, N.; Ibrahim, M.; Spiro, T. G.; Groves, J. T. Trans-dioxo Manganese(V) Porphyrins. *J. Am. Chem. Soc.* **2007**, *129*, 12416−12417.

(26) Pecoraro, V. L.; Baldwin, M. J.; Gelasco, A. Interaction of Manganese with Dioxygen and Its Reduced Derivatives. *Chem. Rev.* **1994**, *94*, 807−826.

(27) Limburg, J.; Vrettos, J. S.; Liable-Sands, L. M.; Rheingold, A. L.; Crabtree, R. H.; Brudvig, G. W. A Functional Model for O−O Bond Formation by the O$_2$-Evolving Complex in Photosystem II. *Science* **1999**, *283*, 1524−1527.

(28) Kim, S. H.; Park, H.; Seo, M. S.; Kubo, M.; Ogura, T.; Klajn, J.; Gryko, D. T.; Valentine, J. S.; Nam, W. Reversible O-O Bond Cleavage and Formation between Mn(IV)-Peroxo and Mn(V)-Oxo Corroles. *J. Am. Chem. Soc.* **2010**, *132*, 14030−14032.

(29) Tsui, E. Y.; Tran, R.; Yano, J.; Agapie, T. Redox-inactive metals modulate the reduction potential in heterometallic manganese−oxido clusters. *Nat. Chem.* **2013**, *5*, 293−299.

(30) Coggins, M. K.; Martin-Diaconescu, V.; De Beer, S.; Kovacs, J. A. Correlation Between Structural, Spectroscopic, and Reactivity Properties Within a Series of Structurally Analogous Metastable Manganese(III)-Alkylperoxo Complexes. *J. Am. Chem. Soc.* **2013**, *135*, 4260−4272.

(31) Coggins, M. K.; Kovacs, J. A. Structural and Spectroscopic Characterization of Metastable Thiolate-Ligated Manganese(III)-Alkylperoxo Species. *J. Am. Chem. Soc.* **2011**, *133*, 12470−12473.

(32) Seo, M. S.; Kim, J. Y.; Annaraj, J.; Kim, Y.; Lee, Y.-M.; Kim, S.-J.; Kim, J.; Nam, W. [Mn(tmc)(O2)]+: A Side-On Peroxido Manganese-(III) Complex Bearing a Non-Heme Ligand. *Angew. Chem., Int. Ed.* **2007**, *46*, 377−380.

(33) VanAtta, R. B.; Strouse, C. E.; Hanson, L. K.; Valentine, J. S. [Peroxotetraphenyl porphinato]manganese(III) and [Chlorotetraphenylporphinato]manganese(II) Anions. Syntheses, Crystal Structures, and Electronic Structures. *J. Am. Chem. Soc.* **1987**, *109*, 1425−1434.

(34) Kitajima, N.; Komatsuzaki, H.; Hikichi, S.; Osawa, M.; Moro-oka, Y. A Monomeric Side-On Peroxo Manganese(III) Complex: Mn(O$_2$)(3,5-^{i}Pr$_2$pzH) (HB(3,5-^{i}Pr$_2$pz)$_3$). *J. Am. Chem. Soc.* **1994**, *116*, 11596−11597.

(35) Singh, U. P.; Sharma, A. K.; Hikichi, S.; Komatsuzaki, H.; Moro-oka, Y.; Akita, M. Hydrogen bonding interaction between imidazolyl N−H group and peroxide: Stabilization of Mn(III)-peroxo complexTp^{i}Pr$_2$Mn(μ^2-O$_2$) (imMeH) (imMeH = 2-methylimidazole). *Inorg. Chim. Acta* **2006**, *359*, 4407−4411.

(36) So, H.; Park, Y. J.; Cho, K.-B.; Lee, Y.-M.; Seo, M. S.; Cho, J.; Sarangi, R.; Nam, W. Spectroscopic Characterization and Reactivity Studies of a Mononuclear Nonheme Mn(III)−Hydroperoxo Complex. *J. Am. Chem. Soc.* **2014**, *136*, 12229−12232.

(37) Shearer, J.; Scarrow, R. C.; Kovacs, J. A. Synthetic models for the cysteinate−ligated Non−Heme Iron Enzyme Superoxide Reductase: Observation and Structural characterization by XAS of an FeIII−OOH Intermediate. *J. Am. Chem. Soc.* **2002**, *124*, 11709−11717.

(38) Kitagawa, T.; Dey, A.; Lugo-Mas, P.; Benedict, J.; Kaminsky, W.; Solomon, E.; Kovacs, J. A. A Functional Model for the Metalloenzyme Superoxide Reductase. *J. Am. Chem. Soc.* **2006**, *128*, 14448−14449.

(39) Nam, E.; Alokolaro, P. E.; Swartz, R. D.; Gleaves, M. C.; Pikul, J.; Kovacs, J. A. An Investigation of the Mechanism of Formation of a Thiolate-Ligated Fe(III)-OOH. *Inorg. Chem.* **2011**, *50*, 1592−1602.

(40) Villar-Acevedo, G.; Nam, E.; Fitch, S.; Benedict, J.; Freudenthal, J.; Kaminsky, W.; Kovacs, J. A. Influence of Thiolate Ligands on Reductive N−O Bond Activation. Oxidative Addition of NO to a Biomimetic SOR Analogue, and its Proton-Dependent Reduction of Nitrite. *J. Am. Chem. Soc.* **2011**, *133*, 1419−1427.

(41) Coggins, M. K.; Toledo, S.; Shaffer, E.; Kaminsky, W.; Shearer, J.; Kovacs, J. A. Characterization and Dioxygen Reactivity of a New Series of Coordinatively Unsaturated Thiolate-Ligated Manganese(II) Complexes. *Inorg. Chem.* **2012**, *51*, 6633−6644.

(42) Bhula, R.; Gainsford, G. J.; Weatherburn, D. C. A New Model for the Oxygen-Evolving Complex in Photosynthesis. A Trinuclear μ_3-Oxo Manganese(III) Complex Which Contains a μ-Peroxo Group. *J. Am. Chem. Soc.* **1988**, *110*, 7550−7552.

(43) Pollock, C. J.; Grubel, K.; Holland, P. L.; DeBeer, S. Experimentally Quantifying Small-Molecule Bond Activation Using Valence-to-Core X-ray Emission Spectroscopy. *J. Am. Chem. Soc.* **2013**, *135*, 11803−11808.

(44) Coggins, M. K.; Toledo, S.; Kovacs, J. A. Isolation and Characterization of an Unsupported, Hydroxo-Bridged Iron(III,III)(μ-OH)$_2$ Diamond Core Derived from Dioxygen. *Inorg. Chem.* **2013**, *52*, 13325−13331.

(45) Coggins, M. K.; Brines, L. M.; Kovacs, J. A. Synthesis and Structural Characterization of a Series of Mn(III)-OR Complexes, Including a Water-Soluble Mn(III)-OH that Promotes Aerobic Hydrogen Atom Transfer. *Inorg. Chem.* **2013**, *52*, 12383−12393.

(46) Popp, B. V.; Stahl, S. S. Oxidatively Induced" Reductive Elimination of Dioxygen from an η2 Peroxopalladium(II) Complex Promoted by Electron-Deficient Alkenes. *J. Am. Chem. Soc.* **2006**, *128*, 2804−2805.

(47) Haumann, M.; Muller, C.; Barra, M.; Grabolle, M.; Dau, H. Photosynthetic O$_2$ Formation Tracked by Time-Resolved X-ray Experiments. *Science* **2005**, *310*, 1019−1021.